Vietnam Academy of Science and Technology

Vietnam Journal of Marine Science and Technology

journal homepage: vjs.ac.vn/index.php/jmst

Characteristics of suspended sediment concentration and distribution of maximum coastal turbidity of the Mekong river

Nguyen Ngoc Tien

Institute of Marine Geology and Geophysics, VAST, Vietnam

Received: 29 December 2022; Accepted: 9 April 2023

ABSTRACT

This paper presents the results of applying a 3D mathematical model to study the in the Mekong riverside area's maximum turbidity zone (MTZ). This study has established and calibrated a three-dimensional system model with a combination of hydraulics-waves and suspended sediment transport with measured data in the study area. Based on the calculated scenarios for the flood and the dry seasons, the results show the occurrence of MTZs in the riparian zone of the Mekong river with typical suspended sediment concentrations (SSC) ranging from 0.04–1.0 kg/m^3 dry season and 0.2–1.1 kg/m^3 flood season. The location and size of the MTZs change seasonally with the interaction between freshwater and tidal oscillations. They appear more in the dry season. At high tide, seawater with high salinity intrudes into estuaries with a range of up to 50 km, causing disturbance and flocculation. While in the flood season, the distribution of the largest turbidity has moved the floodplain with a range of about 20 km.

Keywords: Maximum turbidity, transport of suspended sediment, Mekong river.

Corresponding author at: Institute of Marine Geology and Geophysics, 18 Hoang Quoc Viet, Cau Giay, Hanoi, Vietnam.
E-mail addresses: nntien@imgg.vast.vn

https://doi.org/10.15625/1859-3097/18633
ISSN 1859-3097; e-ISSN 2815-5904/

INTRODUCTION

Maximum turbidity zone (MTZ) in estuaries are features in some coastal estuaries where large amounts of suspended sediment are concentrated. At the maximum turbidity of the estuary, the suspended sediment concentration is higher than elsewhere along the freshwater-sea water transition within the coastal estuary [1]. However, the studies related to MTZ in this area are relatively new. The maximum turbidity area is described by the higher-than-normal variable suspended sediment content when compared to inside the river and outside the coastal area.

The maximum turbidity zone in the estuary is formed and exists due to the interaction between river discharge, tidal dynamics, and gravity [2]. The concentration of suspended sediments (TLL) in the estuary's maximum turbidity zone varies with tidal time and seasonal time scale [3]. When saline water enters the estuary and forms a salt wedge, fine sediments from the river are carried out as small flocs. When these small flocs meet with salt water, these flocs increase due to the sudden change in salinity and the convergence of the flow below the salt wedge. The combination of asymmetric tidal flow and increased precipitation of sediment concentration forms the zone of maximum turbidity (Figure 1) [4, 5]. The formation and movement of the maximum turbidity zone at the estuary is a complex process between dynamic, geological, and hydrological processes [6]. They depend on dynamics of river-sea interactions, sediment discharge, erosion, or deposition of suspended sediments as well as re-suspension of bottom sediments and fluctuations (space, time, etc.) of salinity with tidal influence [7, 8].

The location of the MTZ depends on the river-sea interaction. They move deeper into the river if fresh water is weak (in the dry season) and move downstream when the river water is more vital, as during the rainy season [9–13]. The change in suspended sediment content (TLL) in the MTZ occurs rapidly due to anthropogenic factors [14–16]. Therefore, identifying the mechanism and extent of MTZ can help us understand the characteristics of the LLL in estuaries and intertidal flats.

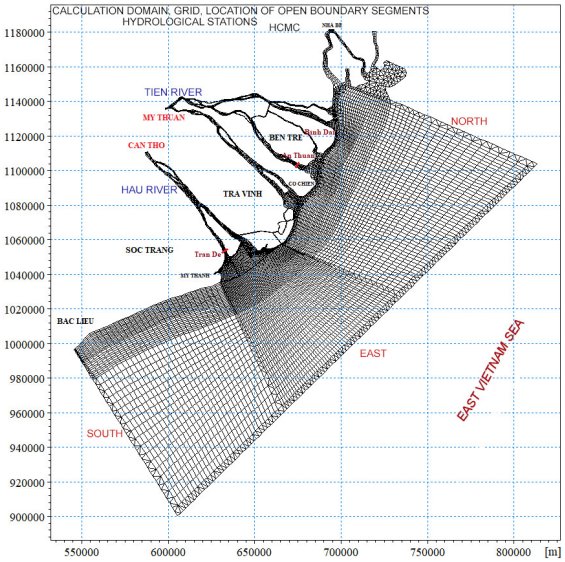

Figure 1. The grid and scope of the study

Some researchers on both models have studied the physical basis for forming the maximum turbidity of the estuary. Firstly, using a model to study the mechanism for maximum turbidity stability applied in estuaries [17]. Second, using analytical and numerical models to study the influence of gravity and tidal forces and the interaction between currents and seabed on the maximum turbidity area [18]. Some research results have applied numerical models [19–21] to evaluate the formation and distribution of the maximum turbidity in the Mekong estuary and some coastal estuaries in South Vietnam.

In the river-sawn area along the Mekong river [19], the occurrence of highly turbid water areas with a typical suspended sediment content of 0.04–0.07 kg/m^3 (dry season) and 0.05–0. 1 kg/m^3 (flood season). The location of the MTZs is about 12–22 km from the river mouths (dry season) and 5–15 km (flood season). The location and extent of these MTZs fluctuate mainly depending on the interaction of the discharge river water masses and tidal water fluctuations. The maximum turbidity areas appear more in the dry season and the time of high water - high tide phase at different locations inside the estuaries.

Salt wedges exist all year round in the Hau river estuary area [20], but their position and

length change depending on the hydrological season, tidal phase, and continuous changes in space and time. In the flood season, their length is short, about 15 km to 25 km, the longest is in the ebb tide phase, and the shortest is in the high tide, distributed from the river mouth to the delta. In contrast, in the dry season, their length is about 50 km during ebb tide, decreasing during high tide.

In some coastal estuaries in Vietnam, the size and location of the maximum turbidity in the Bach Dang estuary [21] constantly changes according to the influence of the seasonal and seasonal material flows from the mainland to the sea tidal water level fluctuations. The location of the most extreme turbidity is about 15 km from shore during low tide during the rainy season, and they are small in scale, appearing closer to shore during the dry season. In addition, according to the analysis of six cross-sectional data at the mouth of the Cam - Nam Trieu rivers [22] during high tide, two mechanisms formed the maximum turbidity. (1) High turbidity exists in the surface layer where salinity ranges from 0.1–1 g/L; (2) The maximum turbid water with lower concentration exists in the bottom layer where the salinity ranges from 1–1 5 g/L. Their length depends on the length of the salt wedge and the magnitude of the rising or falling tides.

Because the Mekong is an extensive river system, the annual flow of water and sediment from the mainland to the estuary is quite large combined with the irregular semi-diurnal tide regime, hydrodynamic-sedimentary conditions occur quite complex and favorable for the occurrence of highly turbid waters. At Dinh An estuary, the amount of sediment is about 0.5 m/month in the flood season and 0.3 m/month in the dry season, which not only causes channel accretion but also creates sandbanks. Based on the application of three-dimensional mathematical modeling tools, using survey data and published results of the author himself in the Hau river area [20], this article will provide additional modeling mechanisms and distribution of maximum turbidity water in other estuaries of the lower Mekong River, assessment of characteristics of suspended sediment concentration, and distribution of maximum coastal turbidity in the Mekong river.

MATERIALS AND METHODS

Materials

Input data sources to establish the baseline and initial shoreline of the calculated domain include: (1) Coastal topographic map at scale 1:5,000, UTM projection grid, 105^o and 108^o axis meridians of 3^o projection, coordinate system VN-2000 national altitude and altitude in 2009 provided by the National Center for Remote Sensing; (2) Topographic measurement data of the river bed and Hau river mouth includes 16 items at the ratio 1:500 to 1:20,000 UTM projection grid, axis meridian 105^o, zone 3^o, coordinate system VN-2000 performed 2009 [23]; (3) Topographical data of the Cuu Long estuaries and surrounding areas in 2009 at the scale of 1:10,000 of the General Department of Water Resources; (4) Hydrographic data of Quan Chanh Bo canal and Mekong river in 2008 at 1:20,000 scale, funded by the Mekong river Commission; (5) Vietnam sea topographic data at scale 1:50,000 and 1:100,000, coordinate system, national elevation VN-2000, meridian 1050 by the Center for Marine Geodetic Surveying in 2009; (6) Topographic data of the main tributaries of the Mekong river, Soai Rap river, Long Tau river, and Cai Mep river are morphological change monitoring datasets produced by the Institute of Marine Engineering and the Southern Institute of Irrigation Science, carried out since 2009, as well as the river cross-section data inherited from the projects and projects by the Ministry of Agriculture and Rural Development.

The latest GIS maps, Landsat, Apot, and Google satellite images define the domain’s coastlines.

The topographic data from the above sources with different reference systems and axis meridians are converted to the UTM - WGS1984, Zone 48 reference systems using FME Quick Translator (FME - Feature Manipulation Engine) data conversion software.

The data source for creating the wind field database is reanalyzed wind data collected from the website: https://cds.climate.copernicus.eu/cdsapp#!/dataset/reanalysis-era5-pressure-levels?tab=form.

Temperature and salinity data in the Mekong estuaries and the ocean are collected from the results of related studies in the same area and the WOA13 database with a resolution of 0.25 [24].

River water discharge and suspended sediment concentration observed from 2008 to 2011 at Can Tho and My Thuan stations were used to develop boundary data.

Actual water levels measured at Tran De, My Thanh, Binh Dai, An Thuan, and Ben Trai stations (Figure 1) are provided by the Vietnam Hydrometeorological Center.

Methods

In this study, the mathematical modeling method was applied. The research results are calculated based on the MIKE 21/3 integrated model (developed by the Danish Hydraulic Institute - DHI) with the domain boundary extended to all Mekong tributaries and the entire Southeastern sea area. The model is integrated from three main modules, including (1) 3-D Hydrodynamic Module - MIKE 3D HD (Hydrodynamics) to determine the water level field, 3D flow, and 3D salinity taking into account the influence of waves and changes in bottom-shore morphology; (2) The MIKE SW (Spectral Wave) wave spectrum module to determine the wave spectrum field taking into account the effects of water level fluctuations, currents and changes in bottom-shore morphology and river-sea processes; (3) The MIKE 3D MT (Mud transport) cohesive sludge transport module and the transformation of the seabed-banks morphology because the cohesive sediment transport is solved by the finite volume algorithm approximating by the flexibility network combining triangular and tetragonal molecules with the number of differential equations with different partials including nine equations for each layer of Sigma, one morphological simulation equation and one wave spectrum effect equation [25, 26].

The mesh is created using the Mesh Generator tool using two types of meshes, triangular and polygonal, with nearly 15 thousand elements and more than 15 thousand nodes. In deep water areas, use a quadrilateral grid with sufficient mesh density to simulate the continuity of the processes to be modeled with the grid cell edge length here, 2–8 km. River tributaries include islets, covered by quadrilateral grids with short sides from 10–100 m across the river and long sides from 200–3,000 m along the river. Triangular grids are used when quad grids cannot be used and are often used for areas with complex shore and bottom topography: estuaries, river crossings, and winding shorelines. Dimensions of the sides of the triangle are 10–2,000 m.

The grid cells are usually arranged so that the short edges have a direction parallel to the normal of the iso-depth line, and the long side has a direction parallel to the iso-depth to increase accuracy in the topographic approximation. In contrast, the number of cells on the net increased insignificantly. In the estuary area, the density of grid cells is high, ensuring a complete approximation of the topographical structure at a scale of 1:10,000. The minor grid edge is 10 m, and the average for the study area is 50 m (Figure 2).

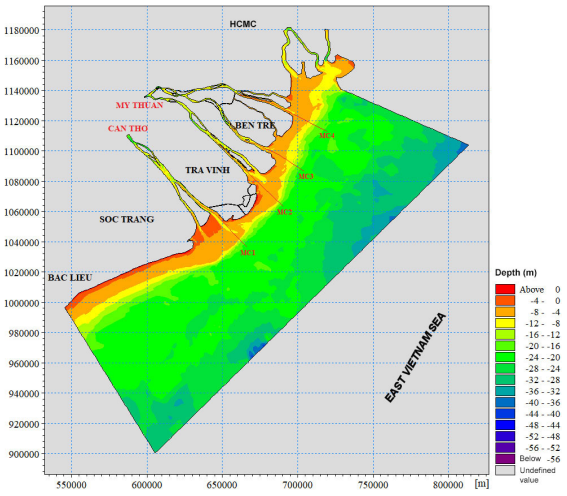

Figure 2. The topography of the study area

Vertically, there are eight layers used with sigma coordinates. The model framework covers the area from coastal Vung Tau in the Northeast to near Ganh Hao coast in the Southwest part. The model has five river borders, including Nha Be, Thi Vai, My Thanh, My Thuan, and Can Tho (Fig. 1). Nha Be and Thi Vai are in the Northeast of the study and belong to the Dong Nai-Saigon

rivers basin. The water flow margin across the Can Tho and My Thuan bridge sections is the hourly discharge measured from 2008 to 2011. The water level margin at the Nha Be section is the actual measured data from 2008 to 2011, the water level margin and velocity. Synthetic currents due to hourly tides and winds at three open boundary segments of the North, East, and South seas are the results extracted from the MIKE 21/3 integrated model simulating HD and SW fields for the entire East Vietnam Sea. The range of suspended sediment concentrations (SSC) at the Can Tho bridge and My Thuan bridge cross-sections is daily SSC from 2008 to 2011. They are separated into two parts: The very fine part consisting of clay particles, rarely accreting as individual particles, account for 50%; and the dust, accounting for 50%.

According to the linear method, the SSC gradient at all three open boundary segments connecting to the ocean is 0. The river cross section at Nha Be and Cai Lon, using natural boundary conditions of the form: SSC gradient according to the linear method, has intersection values ranging from 0.04 kg/m^3 to 0.14 kg/m^3. At each river boundary, the same SSC values are used for all longitudinal layers [27]. The average values of temperature and salinity of water at the Can Tho and My Thuan cross-sections T = 27.5^{o}C; S = 0; At Nha Be, Thi Vai, My Thanh, the hourly measured salinity varies with time, remaining constant along the boundary with the corresponding value (T = 28^{o}C, S about 0–7 g/L; T = 28^{o}C, S about 10–24 g/L; T = 29^{o}C, S range about 6–22 g/L).

There are three open sea borders: North, East, and South (Fig. 1). Seawater temperature and salinity values are assigned (T = 28^{o}C, S = 34 psu). The measured water level elevations at Tran De, Ben Trai, An Thuan, and Binh Dai stations (location in Figure 1) were used to calibrate and verify the model. In addition, the sea level measured near the coast is analyzed to determine the harmonic constants of 8 tidal components (M2, S2, K2, N2, O1, K1, P1, Q1) for use at the boundary's sea in the grid. The offshore tidal constants were extracted from FES2014 [28, 29]. The wave module is set up with a combination of hydrodynamic modeling and sludge transport. The open boundary conditions of the wave model are extracted from the wave climate [30].

The spatial distribution of the roughness height coefficient with values between 20–53 mm was used to establish the layer resistance in this study, and the layer roughness with values in 0.001–0.002 m [31, 32]. The horizontal vortex viscosity is the Smagorinsky formula with a constant value of 0.5. The formula specifies the vertical vortex viscosity; the vortex viscosity is defined as a function of the chaotic kinetic energy (TKE), *k*, and the dissipation of TKE. Two additional transport equations must be solved for TKE and TKE dissipation [33]. The roots of these equations are automatically called up.

The model calibrated with the stability criterion for digital algorithms using the current scheme must satisfy that the *CFL* number (Courant Friedrich Levy) is always less than 1 for all integrated modules into the MIKE 21/3 integration model. Specifically, for the hydrodynamic modulus, the *CFL* number of each mesh element is defined:

$$CFL_{HD} = \left(\sqrt{gh} + |u|\right)\frac{\Delta t}{\Delta x} + \left(\sqrt{gh} + |v|\right)\frac{\Delta t}{\Delta x} + |\mathrm{w}|\frac{\Delta t}{\Delta z} < 1$$

where: h is the depth of the water column; *u*, *v*, *w* are the velocity components along the *x*, *y*, and *z* axes, respectively; g is the acceleration due to gravity; Δx, Δy, Δz are the characteristic lengths of the mesh step of each mesh element, and Δt is the step in time (Δx, Δy are approximately equal to the element's smallest side length, Δz). is the thickness between sigma layers).

For the load modulus of scalar quantities (salinity, suspended sediment, turbulent kinetic energy, turbulent kinetic energy dissipation rate, etc.), the *CFL* number of each calculated mesh element is defined:

$$CFL_{AD} = |u|\frac{\Delta t}{\Delta x} + |v|\frac{\Delta t}{\Delta x} + |\mathrm{w}|\frac{\Delta t}{\Delta z} < 1$$

For the spectrum modulus, the *CFL* number of each grid element is defined:

$$CFL_{sw} = \left|c_x \frac{\Delta t}{\Delta x}\right| + \left|c_y \frac{\Delta t}{\Delta y}\right| + \left|c_\sigma \frac{\Delta t}{\Delta \sigma}\right| + \left|c_\theta \frac{\Delta t}{\Delta \theta}\right| < 1$$

where: c_x and c_y are wave phase velocity along the axes (x, y); c_σ and c_θ are the wave spectrum energy transfer velocity in frequency σ and wave direction θ; and $\Delta\sigma$ and $\Delta\theta$ is the grid step in frequency and direction.

Table 1. Mike 3 HD model parameters

Parameter name	Value or selection value
3-D hydrodynamic model	
Solving technique	Low-level, fast calculated
Calculation step	3 sec
Calculation period	9,264 hours starting from 11/12/2008 to 31/12/2009
Horizontal tangle	Coefficient of tangled viscosity according to Smagorinsky's formula = 0,28
Vertical tangled	Logarithmic formula
Bottom resistance	Rough altitude
The impact of the wind	Reanalyzed wind data were collected from the website https://cds.climate.copernicus.eu/cdsapp#!/dataset/reanalysis-era5-pressure-levels?tab=form
Open boundary in My Thuan and Can Tho	Actual hourly flow rate
Open boundary in Nha Be and My Thanh	Actual hourly water level
Open boundary to the North, East, South	The combined water level due to tides and winds is calculated by the MIKE 21/3 integration model for the entire East Vietnam Sea and then extracted at open boundary
Vertical resolution	8 layers of Sigma, with boroclinic effect due to the influence of salinity
The effect of waves on the flow	Integration with the results of running the MIKE SW model concurrently
Three-dimensional salt transport and diffusion parameters	
Solving technique	Low-level, fast calculation
Horizontal scattering	Calculated according to tangled viscous, scaling factor = 0.3
Vertical scattering	Calculated according to tangled viscous, scaling factor = 0.02
Initial salinity	Fresh water in the river and salt in the sea
Open boundary in My Thuan and Can Tho	Fresh water year round
Open boundary in Nha Be	Rainy season: Fresh water; Dry season: salt (Change by month of the year from 0 to 6 g/L
Open boundary in My Thanh	Change by month of the year (Rainy season: 5 g/L; Dry season: 20 g/L)
Open boundary to the North, East, South	The salinity is 34 g/L
Bottom topography	Updated via integration with concurrent running results of MIKE 3D MT model

Table 2. Parameters of the MIKE 3 FM MT mud transport model

Model parameters	Value to choose to use
Choose parameters	Particle number: 2 (lightning and dust) Number of bottom layers: 2 layers (layer 1: slurry; layer 2: tight mud)
Solving technique	Low-level, fast calculation
Parameters in the water column	
Fall rate coefficient of the 1-lightning component	Spatial variability; taking into account flocculation
Fall rate coefficient of the 2-dust component	Spatial variability; taking into account flocculation
Critical stress begins to deposit 1-clay component	Spatial variability; taking into account flocculation
Critical stress begins to deposit 2-dust component	Spatial variability; taking into account flocculation
Horizontal scattering of components 1 and 2	Proportional to the horizontal turbulent viscosity coefficient with a scaling factor of 0.25
Vertical scattering of components 1 and 2	Proportional to the horizontal turbulent viscosity coefficient with a scaling factor of 0.5
Parameters related to bottom erosion and waterline	
Erosion coefficient of layer 1	Spatial variability
Critical stress at the beginning of layer 1 erosion	Spatial variability
Exponent erosion coefficient of layer 1	8.3
Density of bottom mud layer 1	180 kg/m^3
Erosion coefficient of layer 2	Spatial variability
Critical stress at the beginning of layer 2 erosion	Spatial variability
Exponent erosion coefficient of layer 2	1
Density of bottom mud layer 2	400 kg/m^3
Bottom roughness	Spatial variability
Viscosity and density of water	Update for 3D hydrodynamic model
Original SSC component 1	0.03 kg/m^3
Original SSC component 2	0.02 kg/m^3
Initial thickness of layer 1	0.01 m
Initial thickness of layer 2	0.1 m
Compression speed	0.0001 kg/m^2/s
Clay and dust composition in layer 1	50%, 50%
Clay and dust composition in layer 2	50%, 50%
Open boundary of suspended sediment content (SSC) at the open boundary are Can Tho and My Thuan bridges	Actual data measured daily for the period from 2008 to 2011
Open boundary of SSC in Nha Be and My Thanh	Estimated average monthly figures for the period from 2008 to 2011
SSC opening boundaries at sea North, East, South	Zero Gradient (Neymman conditions)
Morphological	Updating bottom and shore topography

For each grid cell with given input databases and simulation time, Δt is the only parameter that can be changed during model calibration such that the above *CFL* must be less than 1 for all parts. element of the grid and every instant of the entire computation time. This is the most important job of the model calibration step.

In the MIKE 21/3 integration model, the default value of the *CFL* is 0.8 which provides the user with the minimum and maximum *t* values, and an automatic numerical algorithm to set the calculation time step. most reasonable. The parameters and simulation time of the model are shown in Tables 1 and 2.

Calibrate and check the calculated results of the model.

One can use many methods to evaluate the fit between the calculated process curve and the actual measurement. The mean square error criterion can be used by calculating the Sutcliffe-Nash coefficient. The standard of mean square error is calculated by the ratio S/σ with:

$$\sigma = \sqrt{\frac{\sum_{t=1}^{n}\left(Q_{td} - \bar{Q}_{td}\right)^2}{n}}$$ mean square error over the real series;

$$S = \sqrt{\frac{\sum_{t=1}^{n}\left(Q_{tt} - Q_{td}\right)^2}{n}}$$ squared error between real measured and calculated;

Q, $\bar{Q}$ - average flow and discharge or water level and average water level in series;

According to the actual calculation, the degree of conformity is acceptable if the value S/σ does not exceed 0.40–0.45.

The appropriateness between the survey measurement data and the calculation is evaluated and checked through the Sutcliffe-Nash coefficient. The Nash coefficient is calculated as follows:

$$\eta = 1 - \frac{\sum_{i=n}^{1}\left(H_{tdi} - H_{tti}\right)^2}{\sum_{i=n}^{1}\left(H_{tdi} - \overline{H}_{tdi}\right)^2}$$

where: H_{tdi}- the actual water level (flow) measured at time *i* (m); H_{tti}- the calculated water level (flow) at time *i* (m); $\bar{H}_{td}$ - the actual average measured water level (flow) (m).

The Nash-Sutcliffe coefficient can be from -∞ to 1. A coefficient of 1 corresponds to a perfect match of the model and the observed data.

The correction of HD module parameters according to the April and September 2009 survey data set will be decisive for the next steps. The parameters to be adjusted include:

Check the reasonableness of the calculation domain, the grid, and the error, if any, in all input databases, the original topographic data in areas where the topographic data is too old, outdated, or missing.

Select the optimal calculation step Δt to ensure the number of *CFL* < 1, if necessary, to correct the grid to speed up the calculation, including correcting the position of the opening and closing boundaries.

Comparing measured data and model calculation results at four stations, Tran De, Ben Trai, An Thuan, and Binh Dai from September 15 to 30, 2009 (Figure 3), are consistent with the calculated results. Evaluation by Nash criterion reached 0.90.

The results compare the SSC content simulated by the MT module (combined with HD module and SW module) with actual data measured at the S12 station (Figure 4) with the following comments: SSC simulation results on aquifers by MT module and measured data are relatively consistent both in SSC value and in tidal phase variation. Assessment by the Nash criterion reached 0.7.

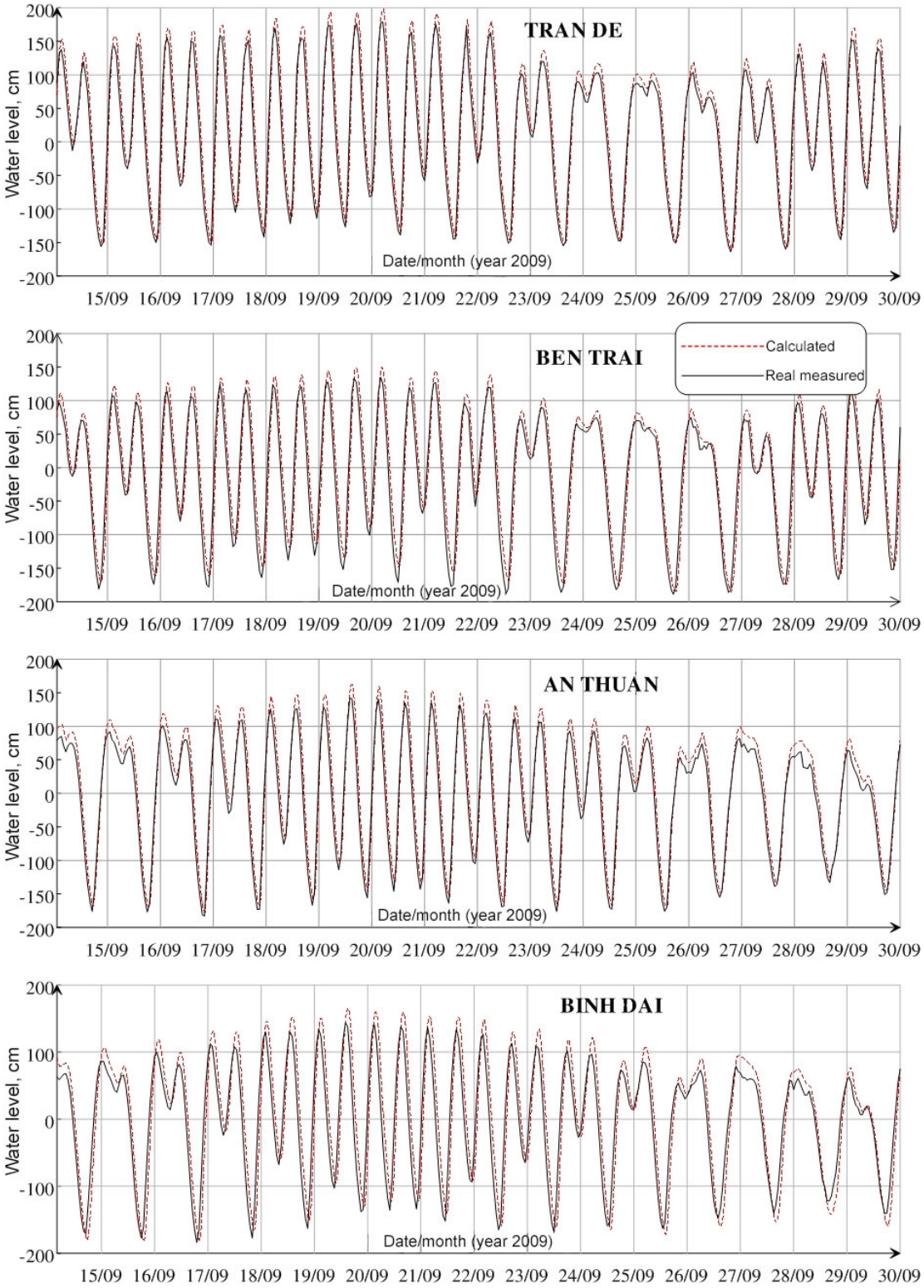

Figure 3. Comparison of simulated and actual results of water level real measured at 4 stations of the Mekong estuary from 15 to 30 September 2009

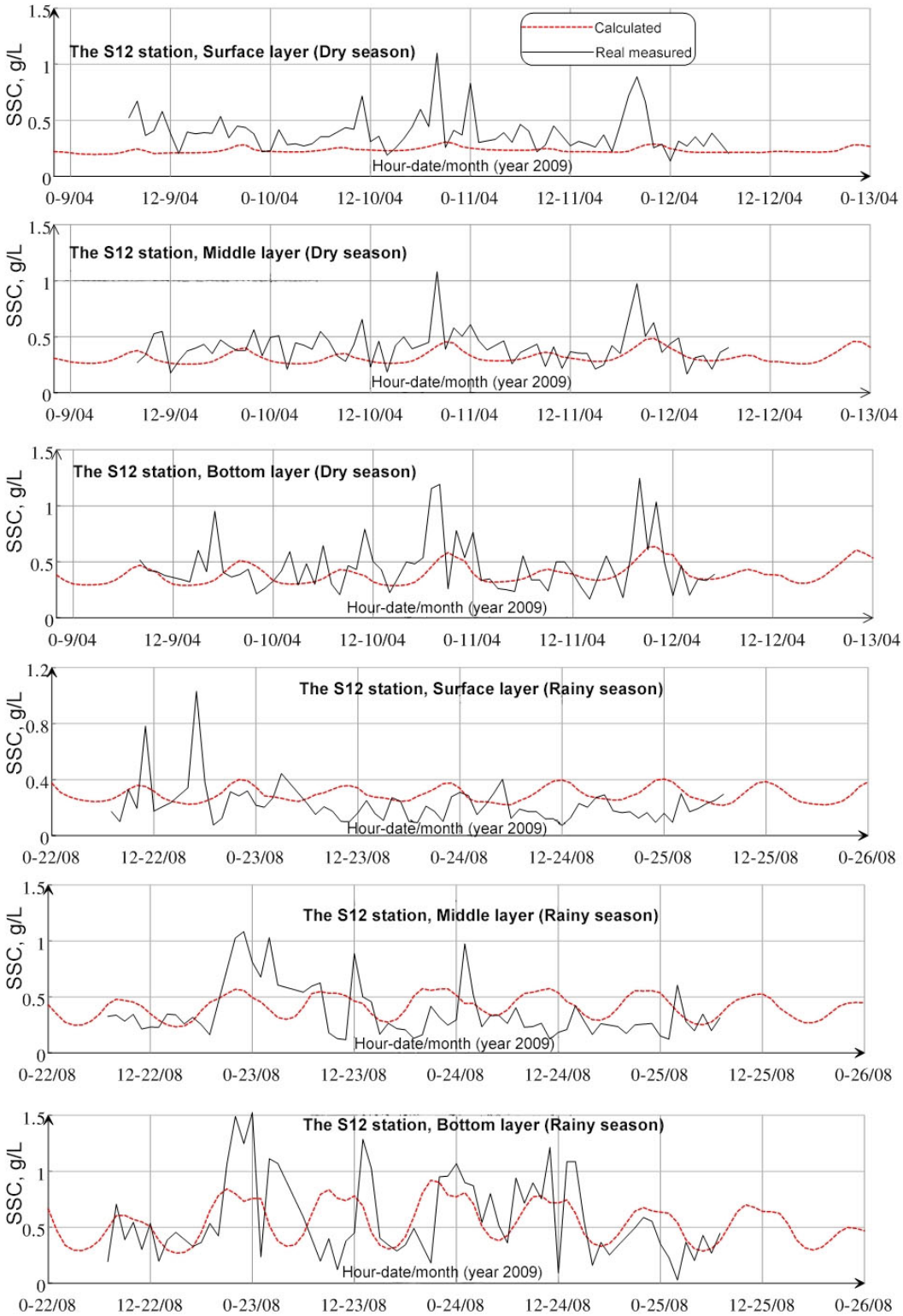

Figure 4. Comparison of simulation results and real measured of SSC the S12 station in April (to verify MT model) and August (to calibrate MT model) in 2009

RESULTS AND DISCUSSION

Spatial distribution of suspended particulate matter in the coastal area of the Mekong river

The results of the MTZ study using computational modeling tools [19–21, 34] indicate that the river-sea dynamics conditions in the coastal areas of the Mekong delta are the formation of the MTZs in the estuaries of this area. The occurrence and size of MTZs are strongly dependent on river discharge and tidal fluctuations. The calculated results also show that, in addition to salt's dynamic mode, distribution characteristics, and thermal structure, the occurrence of MTZ in the Mekong Delta coastal area is related to saltwater distribution. Suspended sediments depend on water level fluctuations and seasonal sediment flow fluctuations from the continent. In the study area, the MTZs appear more in the dry season and the time of the high water - high tide phase at different locations inside the estuaries.

The water's slurry content fluctuation depends most on the regional tidal regime. In the rainy season, the surface layer's suspended sediment concentration (SSC) reaches the highest value of about 0.5 kg/m^3 and is concentrated in the estuaries. The range of suspended sediment concentration with high value is usually located at a depth of 5 m towards the estuary. In the area with a depth of 5m going out, the SSC rarely exceeds 0.02 kg/m^3. This area has a large tidal amplitude, combined with river water discharge, causing a strong tidal flow rate at the time of low tide, strongly affecting the transport of the tidal water offshore (Fig. 5b). In addition, according to previous research results [5], the salinity at this time was pushed to the outside of the estuary. The whole surface layer existed in a freshwater area above and pushed back the saltwater mass layer away. Moreover, the layer of water with salinity ranges from 2–20 g/L distributed about 15 km in the direction perpendicular to the shore. The layer of water with a salt concentration of 8–27 g/L is pushed far beyond the delta slopes. In the dry season, the water flow of small rivers (accounting for about one-third of the water flow in the rainy season) and the large tidal magnitude (over 4.2 m) have created conditions for seawater to penetrate deep into the estuary, causing severe damage to the environment disturbance process. The surface of this disturbed water layer ranges from 5 g/L to 20 g/L; the disturbance range is about 50 km. On the other hand, the flow carrying a small amount of slurry from upstream has caused a significant decrease in the concentration of slurry in the dry season compared to the rainy season, and the scope of impact of the slurry to the water outside the mouth is narrowed. The average calculated value ranges from 0.2 kg/m^3 to 0.3 kg/m^3; the maximum is 0.4 kg/m^3 (Fig. 5a). These results are relatively consistent with previously published results [35–38].

For the middle layer, the results on the distribution of slurry content in the rainy season are precise. Sediment flows from the river are firmly transported to the delta shelf. In the estuary area, the water area with a SSC concentration of about 0.6 kg/m^3 may appear about 25–30 km from the estuary. Water areas with a high suspended sediment concentration above 0.8 kg/m3 exist about 8–10 km from the estuary (Figure 5d). In the dry season, at this tidal phase, the sediment concentration in the middle layer is lower than in the rainy season; the water mass with content from 0.3 kg/m^3 to 0.5 kg/m^3 exists in the estuary area. Inside the river, the SSC is only 0.15–0.2 kg/m^3 (Figure 5c); this may be due to the narrowing of the range of water masses with concentrations from 2 g/L to 20 g/L compared to the surface layer, which represents a stratification of salinity in the deeper water layer. The spreading range of freshwater mass in the low tide phase is much narrower than the surface layer; the water mass with salt concentration from 8–20 g/L predominates. For the dry season, salinity from 5 g/L to 16 g/L still exists inside the river with a length of about 40 km (Dinh An estuary) in this water layer; salt seasoning may exist here until the disturbance process ends [20].

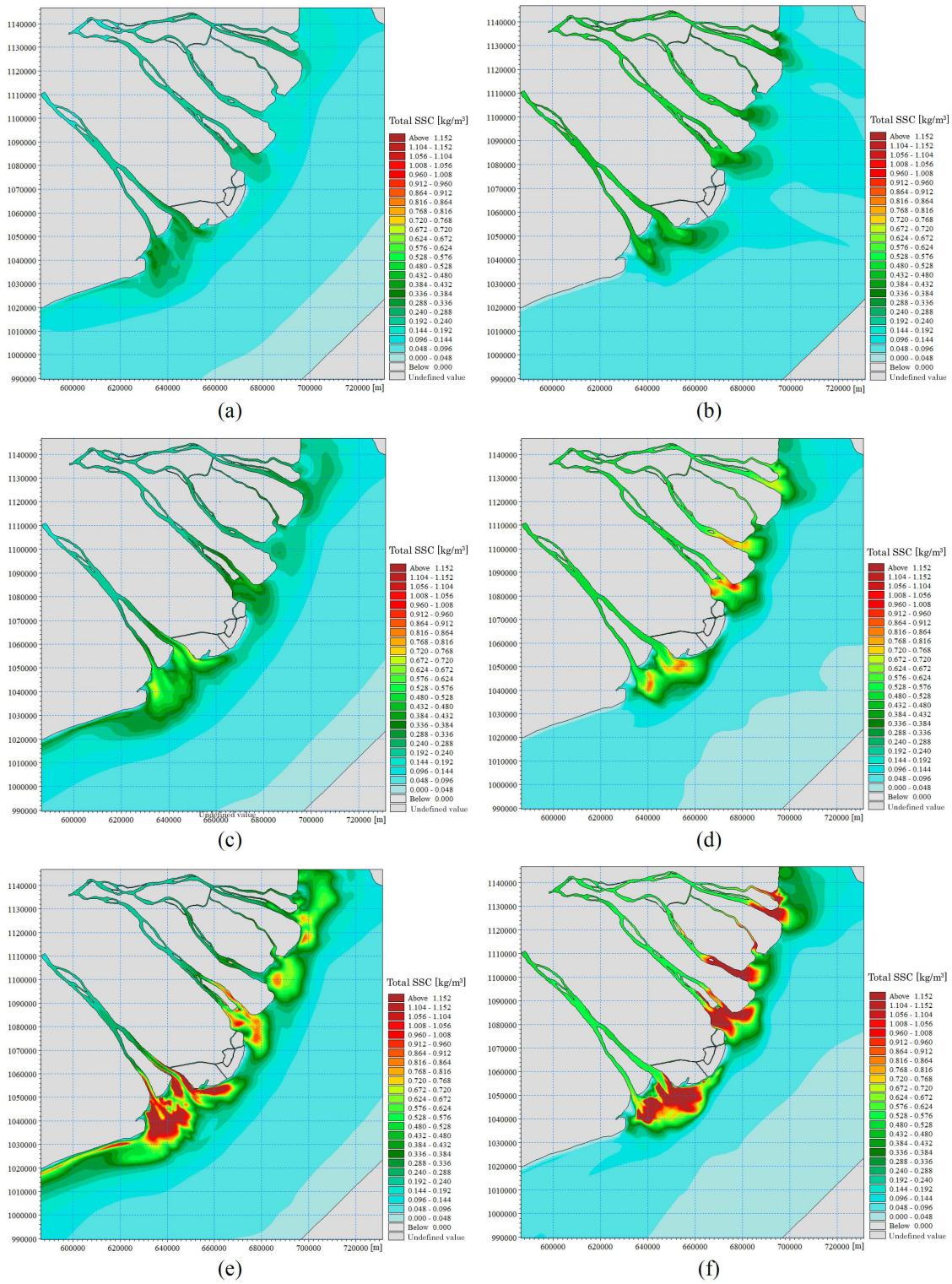

Figure 5. Spatial distribution of suspended sediment according to the seasons at layers: Surface layer (a- dry season, b- rainy season); Middle layer (c- dry season, d- rainy season); Bottom layer (e- dry season, f- rainy season)

At the bottom layer, the simulation results show that the SSC is much higher than that of the middle layer and the surface layer; the value is up to 1.4 kg/m^3 and is concentrated in the estuary (Figures 5e, 5f). The causes for the high concentration of sediment in the bottom layer can be: (1) Due to the interaction between the river and sea water masses forming salt wedges, which facilitate the flocculation and settling of suspended sediments; (2) It is possible that the dynamic process in this area has eroded the bottom, promoted the re-suspended bottom sediment content and contributing to the formation of the maximum turbidity area. In the dry season, when the tide is low, the salt wedge still exists, and the range is about 50 km (according to the results of analysis of survey data), which is an advantage for suspended sediments to flocculate and settle in high-temperature conditions stratification. In addition, the influence of hydrodynamic processes such as wave fields and tidal currents in the water layer close to the bottom has caused erosion and sediment erosion. This phenomenon will increase the SSC here, although lower than in the rainy season, but at a high level from 0.8–1.1 kg/m^3.

In the case of the receding tide phase, the sediment flows from the rivers most rapidly toward the sea. In the case of the high tide phase, while a mass of water with high suspended sediment content from the mainland is still supplied, a mass of saline water with high salinity moves inland. The interaction between these two water bodies during the ebb tide phase causes a significant narrowing of the influence of the water mass carrying suspended sediment from the estuary, making tangled areas appear more prominent.

During the high-water period, the influence of saltwater mass on the continent is most significant. In the rainy season, the water mass with suspended sediment from the river is removed from the estuaries. The interaction between the saline wedge and the flow of suspended particulate matter pushed away by the river flow has contributed to the appearance of some areas of maximum turbulence in the main estuaries of the region. In the dry season, the water mass with suspended sediment content from the continent is not significant; the influence of saline water becomes dominant with the rising tide phase, causing MTZs to appear more profound in the estuaries, and the suspended particulate matter content is much smaller when compared to the rainy season.

Vertical distribution of maximum turbidity according to cross-sections along the banks of the Mekong river

Distribution according to a depth of SSC content at the cross-sections MC1, MC2, MC3, and MC4 (Location in Figure 2) has a length of 60 km. In this study, we calculated, simulated for one year, and extracted the results at low tide to compare with Wolansky's research results in November 1993 and 1996 [35] and Daniel J. Nowacki et al., [38]. The extracted MC1 coincides with the author's published survey stations in 2020 [20].

According to Wolansky's results, the SSC at MC1 only fluctuates in the range of 0.15–0.3 kg/m^3 and is deposited (but very little) at the time of tidal change state (from low tide to high tide) or vice versa). Furthermore, re-suspended when there is a flow rate > 0.5 m/s. The maximum turbidity does not exist in the freshwater area from the Can Tho bridge to the estuary area in the rainy season flow condition. Meanwhile, according to the research results of Daniel J. Nowacki et al., [38], at three cross-sections on the Hau river mouth area. In the area with zero salinity, SSC in this water mass ranges from 0.1 kg/m^3 to 0.2 kg/m^3; in the bottom area, the content reaches 0.4 kg/m^3. Thus at the time of high tide and low tide in the rainy season, a salt wedge is formed with a length of about 20 km; above the salt wedge, the salinity ranges from 0 to 8 g/L, and the bottom wedge of salt at degrees salinity reaches from 10–18 g/L. The SSC in the area where the salt wedge exists ranges from 0.4 g/L to 0.8 g/L; this suspended sediment is deposited at the tide from high tide to recede and re-suspended when there is current speed flow during this ebb tide increases.

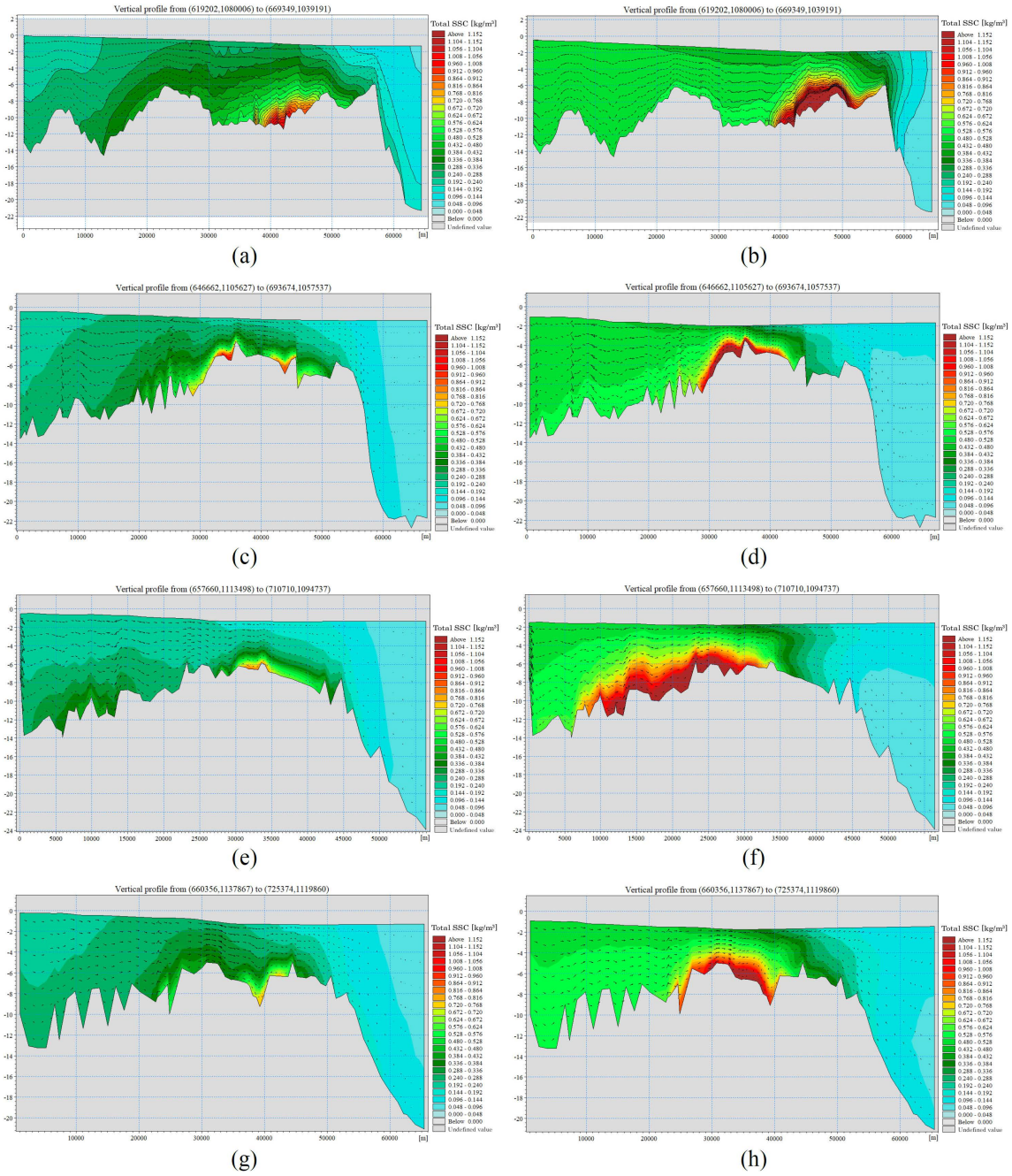

Figure 6. Vertical distribution of solid waste concentration (kg/m^3) on longitudinal section: outside Dinh An river mouth - MC1 (a- dry season, b- rainy season); outside the mouth of Cung Hau river - MC2 (c- dry season, d- rainy season); outside Ham Luong estuary - MC3 (e- dry season, f- rainy season); outside Dai gate - MC4 (g- dry season, h- rainy season) time of low tide

According to the results of this study, the area of salinity change in the dry season and the formation and displacement of salt wedges was determined from Dai Ngai station (5 km from Dai Ngai to the sea) to the estuary area, with 50 km. The reason may be that the river discharge pushes the water with a salinity of 15–20 g/L (previously existing) to the sea, and

because the flow is small this season, a salt wedge is formed here. During the tidal cycle, the water mass with salinity from 15 g/L to 20 g/L still exists in the estuary area. Because the salinity and stratification of salinity in the dry season are much larger than in the rainy season, flocculation and sedimentation occurred more strongly. Sediments from the sea can penetrate deep into the estuary, mix, flocculate, and deposit here. The calculated SSC content at the MC1 cross-section ranges from 0.1–0.3 kg/m^3 in the surface layer to 0.41 kg/m^3 in the middle and bottom layers (Fig. 6a). At MC2, the surface sediment concentration ranges from 0.04 kg/m^3 to 0.2 kg/m^3; the bottom layer is less than 0.9 kg/m^3 (Fig. 6c). At MC3 and MC4, the SSC at the aquifers is smaller than that of MC1; the bottom layer ranges from 0.4 kg/m^3 to 0.6 kg/m^3, and the surface layer is less than 0.1 kg/m^3 (Figs. 6e and 6g).

During the rainy season, the SSC at the MC1, MC2, MC3, and MC4 sections is much higher than that in the dry season at all strata.

The trend of fluctuations and formation of MTZs in the rainy season is similar to the dry season. However, because river dynamics in the wet season are much greater than in the dry season, the properties of the MTZ at the Mekong River sections change significantly compared to the dry season (Figs. 6b, 6d, 6f, and 6h). The changes are:

The MTZ range extends to about 15 km to 20 km. The position of the maximum turbidity water areas in the dry season is shifted closer to the river mouth, about 3–8 km, compared to the flood season, suggesting that the influence of the river-sea interaction process is strong.

The suspended sediment concentration of MTZs in the flood season is higher than in the dry season. At the MC1, MC2, MC3, and MC4 sections, the specific SSC content fluctuates at the surface layer ranging from 0.2–0.5 kg/m^3. For the bottom layer, the SSC ranges from 0.6–1.1 kg/m^3 (Figs. 6b–6h).

The occurrence of MTZs during the flood season in the estuaries of the Mekong river is less frequent than in the dry season, which occurs mainly at high tide and during high water. MTZ also appears less these days, which influences river water, meaning that when the amount of water is very large to reduce the intrusion of salt water into the estuaries, fresh water and suspended matter will move strongly towards the sea and prevent the formation of MTZ in the estuaries.

The analysis results show that the MTZs in estuaries along the banks of the Mekong Delta are strongly dependent on water level fluctuations, sediment supply, and seasonal river water fluctuations. Compared with the Bach Dang estuary [21], the fluctuations of the MTZs (in space and time) between high and low tides in this area are smaller. Due to differences in morphology, and dynamic conditions, the MTZ in the Mekong estuaries appears more clearly than in the estuaries of the Bach Dang river, especially during the late flood and dry seasons. The MTZs in this area are located deep inside the estuary, while at the Bach Dang estuary, most of the MTZs are located outside.

Bottom currents carrying salinity flow inland at some estuaries, while surface flows carry suspended sediments towards the sea. As the surface sediments begin to floc, they settle and are moved back to the mainland at different tidal periods forming turbid water in the estuary area. Due to the asymmetry of the tides and the role of the salinity gradient in maintaining the maximum turbidity of the estuary, this mechanism is present in the Cam - Nam Trieu estuary [22], which is also why the estuary region is turbid. The maximum turbidity in this area is relatively low compared to other estuaries, including the Hau river mouth [20] and estuaries of the Mekong river system [21].

In the flooded delta of the lower Mekong river, the concentration of slurry in the maximum turbidity fluctuates under the influence of current and tidal velocities. When the tidal flow rate in the estuary area and the delta shelf is significant, it will increase and decrease the sediment concentration from the bottom to the surface layer in the water column. The trend of sediment transport and deposition at the time of tide changes from low tide to high tide or vice versa, then re-suspended when the flow rate increases during the high tide phase. The change of direction of the two tidal phases (low tide to high tide) occurs very

quickly. In comparison, the change between the two tidal phases takes 3 hours, which leads to asymmetry of the tidal ellipse and can cause the process of transporting sediment from the delta shelf into the Mekong estuary.

CONCLUSION

The maximum turbidity zone at the Mekong estuaries exists all year round—the barocline effect forms due to saline wedges and the flocculation process of suspended sediments in brackish water. The position almost coincides with the salty wedge tongue's existing position and changes seasonally, according to the tidal phase, and fluctuates strongly in space and time. The impact of waves and tidal currents on suspended and bottom sediment concentrations in the dry season is more significant than in the rainy season. Therefore, the spatial distribution of the maximum turbidity at the Mekong estuary during the dry season is larger than that of the rainy season.

During the dry season, seawater with high salinity accompanied by suspended sediments penetrates deep and exists inside the estuary, causing disturbance and flocculation. The intrusion range is up to 50 km, creating a mass of water with high suspended sediment content from 0.04 kg/m^3 to 1.0 kg/m^3, which is moved in/out by the tidal current up/down for a few kilometers according to the tidal phase. The distribution of the maximum turbidity at the mouths of the Mekong river during the rainy season is shifted to the floodplain shelf in the range of 15 km to 20 km with the SSC ranging from 0.2 kg/m^3 to 1.1 kg/m^3.

Acknowledgments: This research work is funded by funding and survey data by the Project under the Basic Science Development Program in Earth and Marine Sciences for 2017–2025. Subject code: KHCBTĐ.01/20–22. Basic investigation project code: UQĐTCB.03/22–23 and UQ.ĐTCB.03/20–21, supported by topics with code: CP1862.01/20–22 and VAST05.04/22–23.

REFERENCES

[1] Dyer, K. R., 1995. Sediment transport processes in estuaries. In *Developments in Sedimentology* (Vol. 53, pp. 423–449). *Elsevier*. https://doi.org/10.1016/S0070-4571(05)80034-2

[2] Unverricht, D., Szczuciński, W., Stattegger, K., Jagodziński, R., Le, X. T., and Kwong, L. L. W., 2013. Modern sedimentation and morphology of the subaqueous Mekong Delta, Southern Vietnam. *Global and Planetary Change*, *110*, 223–235. https://doi.org/10.1016/j.gloplacha.2012.12.009

[3] Grabemann, I., Uncles, R. J., Krause, G., and Stephens, J. A., 1997. Behaviour of turbidity maxima in the Tamar (UK) and Weser (FRG) estuaries. *Estuarine, Coastal and Shelf Science*, *45*(2), 235–246. doi: 10.1006/ecss.1996.0178

[4] Wolanski, E., King, B., and Galloway, D., 1995. Dynamics of the turbidity maximum in the Fly River estuary, Papua New Guinea. *Estuarine, Coastal and Shelf Science*, *40*(3), 321–337. doi: 10.1016/S0272-7714(05)80013-7

[5] Wolanski, E., Huan, N. N., Nhan, N. H., and Thuy, N. N., 1996. Fine-sediment dynamics in the Mekong River estuary, Vietnam. *Estuarine, Coastal and Shelf Science*, *43*(5), 565–582. https://doi.org/10.1006/ecss.1996.0088

[6] Li, J., and Zhang, C., 1998. Sediment resuspension and implications for turbidity maximum in the Changjiang Estuary. *Marine Geology*, *148*(3–4), 117–124. doi: 10.1016/S0025-3227(98)00003-6

[7] Jay, D. A., and Musiak, J. D., 1994. Particle trapping in estuarine turbidity maxima. *Journal of Geophysical Research*, *99*(20), 446–20.

[8] Sherwood, C. R., Harris, C. K., Geyer, W. R., and Butman, B., 2002. Toward a community coastal sediment transport modeling system: the second workshop. *Eos, Transactions, American Geophysical Union*, *83*(51), 604–605. https://doi.org/10.1029/2002EO000414

[9] Allen, G. P., and Castaing, P., 1973. Suspended sediment transport from the Gironde estuary (France) onto the adjacent continental shelf. *Marine Geology*, *14*(5), 47–53. https://doi.org/10.1016/0025-3227(73)90011-X

[10] Geyer, W. R., Woodruff, J. D., and Traykovski, P., 2001. Sediment transport and trapping in the Hudson river estuary. *Estuaries*, *24*, 670–679. https://doi.org/10.2307/1352875

[11] Sanford, L. P., Suttles, S. E., and Halka, J. P., 2001. Reconsidering the physics of the Chesapeake Bay estuarine turbidity maximum. *Estuaries*, *24*, 655–669. https://doi.org/10.2307/1352874

[12] Uncles, R. J., and Stephens, J. A., 1993. Nature of the turbidity maximum in the Tamar Estuary, UK. *Estuarine, Coastal and Shelf Science*, *36*(5), 413–431. https://doi.org/10.1006/ecss.1993.1025

[13] Diaz, M., Grasso, F., Le Hir, P., Sottolichio, A., Caillaud, M., and Thouvenin, B., 2020. Modeling mud and sand transfers between a macrotidal estuary and the continental shelf: Influence of the sediment transport parameterization. *Journal of Geophysical Research: Oceans*, *125*(4), e2019JC015643. https://doi.org/10.1029/2019JC015643

[14] Yang, Y., Li, Y., Sun, Z., and Fan, Y., 2014. Suspended sediment load in the turbidity maximum zone at the Yangtze River Estuary: The trends and causes. *Journal of Geographical Sciences*, *24*, 129–142. https://doi.org/10.1007/s11442-014-1077-3

[15] Gao, J. H., Jun, L. I., Harry, W. A. N. G., Bai, F. L., Cheng, Y., and Wang, Y. P., 2012. Rapid changes of sediment dynamic processes in Yalu river estuary under anthropogenic impacts. *International Journal of Sediment Research*, *27*(1), 37–49. doi: 10.1016/S1001-6279(12)60014-6

[16] Wan, Y., Roelvink, D., Li, W., Qi, D., and Gu, F., 2014. Observation and modeling of the storm-induced fluid mud dynamics in a muddy-estuarine navigational channel. *Geomorphology*, *217*, 23–36. https://doi.org/10.1016/j.geomorph.2014.03.050

[17] Uncles, R. J., Barton, M. L., and Stephens, J. A., 1994. Seasonal variability of fine-sediment concentrations in the turbidity maximum region of the Tamar Estuary. *Estuarine, Coastal and Shelf Science*, *38*(1), 19–39. https://doi.org/10.1006/ecss.1994.1002

[18] Burchard, H., and Baumert, H., 1998. The formation of estuarine turbidity maxima due to density effects in the salt wedge. A hydrodynamic process study. *Journal of Physical Oceanography*, *28*(2), 309–321. https://doi.org/10.1175/1520-0485(1998)028<0309:TFOETM>2.0.CO;2

[19] Vinh, V. D., Lan, T. D., Tu, T. A., Kim Anh, N. T., 2014. A numerical model to study maximum turbidity zones in Mekong estuary coastal area. *Vietnam Journal of Marine Science and Technology*, *14*(3A), 317–326. doi: 10.15625/1859-3097/14/3A/5208 (in Vietnamese).

[20] Tien, N. N., Cuong, D. H., Mau, L. D., Tung, N. X., and Hung, P. D., 2020. Mechanism of formation and estuarine turbidity maxima in the Hau river mouth. *Water*, *12*(9), 2547. https://doi.org/10.3390/w12092547

[21] Vinh, V. D., Thanh, T. D., 2012. Aplication numerical model to study on maximum turbidity zones in Bach Dang estuary. *Vietnam Journal of Marine Science and Technology*, *12*(3), 1–11. (in Vietnamese).

[22] Duy Vinh, V., Ouillon, S., and Van Uu, D., 2018. Estuarine Turbidity Maxima and variations of aggregate parameters in the Cam-Nam Trieu estuary, North Vietnam, in early wet season. *Water*, *10*(1), 68. doi: 10.3390/w10010068

[23] PortCoast Consultant Corporation, 2006, Feasibility project of Waterway for heavy-tonnages ships to enter the Hau river, Ministry of Transport, Vietnam. (in Vietnamese).

[24] Boyer, T., Ed., Mishonov, A., Technical Ed., 2013. World Ocean Atlas 2013 Product Documentation. *Ocean Climate Laboratory NODC/NESDIS/NOAA. Silver Spring, MD*. http://www.nodc.noaa.gov/OC5/indprod

[25] DHI, 2014. Mike 21/3 Coupled Model FM.

[26] DHI, 2014. Mike 21 & Mike 3 Flow Model FM. Hydrodynamic and Mud Transport Module. *Scientific Documentation.*

[27] DHI, 2014. Mike 21 & Mike 3 Flow Model FM. Mud Transport Module. *Scientific Documentation*.

[28] Lefevre, F., Lyard, F. H., Le Provost, C., and Schrama, E. J., 2002. FES99: a global tide finite element solution assimilating tide gauge and altimetric information. *Journal of Atmospheric and Oceanic Technology*, *19*(9), 1345–1356. https://doi.org/10.1175/1520-0426(2002)019<1345:FAGTFE>2.0.CO;2

[29] Lyard, F., Lefevre, F., Letellier, T., and Francis, O., 2006. Modelling the global ocean tides: modern insights from FES2004. *Ocean dynamics*, *56*, 394–415. https://doi.org/10.1007/s10236-006-0086-x

[30] Argoss, B. M. T., 2011. Overview of the service and validation of the database waveclimate. *Reference: RP_A870*. Available online: www.waveclimate.com; accessed 15 April 2016.

[31] Schneider, V. R., and Arcement, G. J., 1989. Guide for Selecting Manning's Roughness Coefficients for Natural Channels and Flood Plains. *Available from the US Geological Survey, Books and Open-File Reports Section, Box 25425, Federal Center, Denver, CO 80225-0425. Water-Supply Paper 2339, 1989. 38 p, 22 fig, 4 tab, 23 ref.*

[32] Simons, D. B., and Şentürk, F., 1992. Sediment transport technology: water and sediment dynamics. *Water Resources Publication*.

[33] Rodi, W., 1980. Turbulence models and their application in hydraulics-A state of the art review. *NASA STI/Recon Technical Report A*, *81*, 21395.

[34] Lin, J., and Kuo, A. Y., 2003. A model study of turbidity maxima in the York River Estuary, Virginia. *Estuaries*, *26*, 1269–1280. doi: 10.1007/BF02803629

[35] Wolanski, E., Nhan, N. H., and Spagnol, S., 1998. Sediment dynamics during low flow conditions in the Mekong River estuary, Vietnam. *Journal of Coastal Research*, 472–482.

[36] Eidam, E. F., Nittrouer, C. A., Ogston, A. S., DeMaster, D. J., Liu, J. P., Nguyen, T. T., and Nguyen, T. N., 2017. Dynamic controls on shallow clinoform geometry: Mekong Delta, Vietnam. *Continental Shelf Research*, *147*, 165–181. https://doi.org/10.1016/j.csr.2017.06.001

[37] Duy Vinh, V., Ouillon, S., Van Thao, N., and Ngoc Tien, N., 2016. Numerical simulations of suspended sediment dynamics due to seasonal forcing in the Mekong coastal area. *Water*, *8*(6), 255. https://doi.org/10.3390/w8060255

[38] Nowacki, D. J., Ogston, A. S., Nittrouer, C. A., Fricke, A. T., and Van, P. D. T., 2015. Sediment dynamics in the lower M ekong R iver: Transition from tidal river to estuary. *Journal of Geophysical Research: Oceans*, *120*(9), 6363–6383. https://doi.org/10.1002/2015JC010754